Atmospheric Environment 43 (2009) 5056–5067

Contents lists available at ScienceDirect

Atmospheric Environment

journal homepage: www.elsevier.com/locate/atmosenv

Street canyon ventilation and atmospheric turbulence

P. Salizzoni [a,b,*], L. Soulhac [a], P. Mejean [a]

[a] Laboratoire de Mécanique des Fluides et d'Acoustique, Université de Lyon CNRS, École Centrale de Lyon, INSA Lyon, Université Claude Bernard Lyon I 36, avenue Guy de Collongue, 69134 Ecully, France
[b] Dipartimento di Ingegneria Aerospaziale, Politecnico di Torino Corso Duca degli Abruzzi 24, Torino, Italy

ARTICLE INFO

Article history:
Received 20 April 2009
Received in revised form
24 June 2009
Accepted 26 June 2009

Keywords:
Street canyon
Turbulent mass transfer
Urban air pollution
Dispersion models

ABSTRACT

Operational models for pollutant dispersion in urban areas require an estimate of the turbulent transfer between the street canyons and the overlying atmospheric flow. To date, the mechanisms that govern this process remain poorly understood. We have studied the mass exchange between a street canyon and the atmospheric flow above it by means of wind tunnel experiments. Fluid velocities were measured with a Particle Image Velocimetry system and passive scalar concentrations were measured using a Flame Ionisation Detector. The mass-transfer velocity between the canyon and the external flow has been estimated by measuring the cavity wash-out time. A two-box model, used to estimate the transfer velocity for varying dynamical conditions of the external flow, has been used to interpret the experimental data. This study sheds new light on the mechanisms which drive the ventilation of a street canyon and illustrates the influence of the external turbulence on the transfer process.

1. Introduction

Over the last three decades, several models of the mass exchange between a street canyon and the overlying atmospheric flow have been developed to predict pollutant dispersion inside the canyon (Hotchkiss and Harlow, 1973; Johnson et al., 1973; Yamartino and Wiegand, 1987; Berkowicz et al., 1997; Soulhac, 2000). The aim of these models is to compute the spatially averaged concentration of pollutant within a street canyon and the pollutant flux from/to the canyon to/from the atmosphere. An estimate of the transfer velocity – referred to here as u_d – is therefore required. Several studies have attempted to define the dependence of u_d on the dynamical conditions of the external flow and of the canyon geometry. Among these we cite in-situ experiments by DePaul et al. (1985) and Louka et al. (1998), laboratory experiments Barlow et al. (2004), Caton et al. (2003), Narita (2007) and de Paula Gomes et al. (2007) and numerical studies by Solazzo and Britter (2007) and Cai et al. (2008).

These studies all agree that the exchange process is driven by the dynamics of the shear layer at the top of the canyon through the forcing action of the external flow. However, several aspects of the process remain poorly understood, particularly the role of the turbulent structure of the external flow on the dynamics of the shear layer at roof height and therefore on the flow within the canyon. Soulhac (2000) applied theoretical considerations and developed an analytical model. The problem has been also studied numerically by Kim and Baik (2003) and experimentally and theoretically by Caton et al. (2003).

This work seeks to determine the influence of the dynamical conditions of the atmospheric turbulence on the mass transfer between a two-dimensional street canyon of square cross-section and the overlying atmospheric flow. Given that many aspects of the problem remain poorly understood, the study focuses on a simplified model of the urban canopy, made up of a uniform array. Our results could then be further extended to the case of more complex geometries in order to investigate how local inhomogeneities of the building array would modify the process.

Our objective is to determine whether the turbulent transfer is mainly due to turbulence generated locally within the shear layer or to turbulence transported towards the canyon from the external boundary layer flow. In Section 2 we set the fluid dynamical aspects of the problem and review the existing models. In Section 3 we describe our experimental apparatus and techniques. Experimental results are presented in Section 4. The description of the mathematical model adopted to analyse the results is given in Section 5 and a comparison between experimental and theoretical results is provided in Section 6. Conclusions are drawn in Section 7.

* Corresponding author at: Laboratoire de Mécanique des Fluides et d'Acoustique, Université de Lyon CNRS, École Centrale de Lyon, INSA Lyon, Université Claude Bernard Lyon I 36, avenue Guy de Collongue, 69134 Ecully, France. Tel.: +33 4 72186507.
E-mail address: pietro.salizzoni@ec-lyon.fr (P. Salizzoni).

1352-2310/$ – see front matter © 2009 Elsevier Ltd. All rights reserved.
doi:10.1016/j.atmosenv.2009.06.045

2. Theory and previous model

2.1. Theory

The turbulent transfer between a street canyon and the overlying atmospheric flow is an unsteady process characterised by high intermittency. The energy for this process is provided by the mean kinetic energy of the external flow, whose forcing action on the canyon flow is regulated by the dynamics of a region of high shear at the interface between the two. Within this shear layer Kelvin-Helmholtz instabilities arise and generate vortices that grow while they are advected downstream from the upwind corner. The unstable condition of the flow results in a flapping motion of the shear layer and a subsequent intermittent inflow of turbulent structures into the canyon which induces the bulk transfer between the canyon and the external flow. We wish to determine whether the shear layer dynamics are influenced by the structure of the external flow, e.g. the velocity profile, or by locally generated turbulence.

If we consider that the entire process is driven by the dynamics of the shear layer through the forcing action of the external flow, we expect the transfer velocity u_d to scale on $\triangle U$, the mean velocity difference across the shear layer[1]:

$$\frac{u_d}{\Delta U} = \alpha \tag{1}$$

where α must be a function of the canyon geometry and the dynamical conditions of the external flow.

Assuming that the geometry of the canyon is fixed we can then focus on the role of the atmospheric turbulence and consider two limiting hypotheses:

1. the structure of the atmospheric turbulence has negligible influence on the shear layer dynamics so that all velocities in the shear layer scale on $\triangle U$ and

$$\alpha = \text{const} \tag{2}$$

2. the turbulence structure of the external atmospheric boundary layer flow – which can be characterised by a friction velocity u_* and an integral length scale L_e – influences the shear layer dynamics and therefore:

$$\alpha = f\left(\frac{u_*}{\Delta U}; \frac{L_e}{H}\right) \tag{3}$$

Here, H is the canyon height, which is the only characteristic length scale.

2.2. Previous models

Current *operational models* of pollutant dispersion in urban areas describe the mass transfer between the urban canopy and the atmosphere aloft by means of few parameters.

These 'box models' model the canyon as a box with uniform pollutant concentration overlain by a discontinuity surface across which a mass exchange takes place. In these simple models the mean velocity within the cavity is assumed to be zero and the time-averaged velocity profile in the external flow U_1 is assumed to be uniform, so that $\triangle U = U_1$. Equation (1) is then usually written in the form

$$u_d = \alpha U_1 \tag{4}$$

which expresses the idea that the mass transfer depends on the free wind velocity. Numerical values of α differ from one model to the other.

The STREET model (Johnson et al., 1973) follows hypothesis (1) and assumes $\alpha = 1/7$.

Other models adopt hypothesis (2) and define α as a function of the atmospheric turbulence. An example of this is the OSPM model (Berkowicz et al., 1997) which sets

$$\alpha = i$$

where $i = \sigma_{w1}/U_1$ is the turbulence intensity of the external flow, given by the ratio between the r.m.s. of the vertical velocity fluctuation at roof level σ_{w1} and the mean wind velocity at roof level U_1. However, in the OSPM model, i is taken as a fixed value equal to 0.1, which is considered representative of the turbulence intensity in an urban environment.

Other authors define more clearly the dependence of α on the external flow conditions. Hotchkiss and Harlow (1973) assumes that

$$\alpha = \sqrt{\frac{K_m}{U_1 W}}$$

where W is the canyon width and K_m is a turbulent diffusion coefficient. Similarly, in the SIRANE model, Soulhac (2000) assumes that

$$\alpha = \pi\sqrt{\frac{K_m}{U_1 W}}$$

In accordance with Prandtl's mixing length theory, both models express K_m ($= L_e\sigma_w$) as the product of a the integral length scale L_e and the r.m.s. of the vertical fluctuating velocity σ_w in the external flow.

3. Experimental details

3.1. Experimental set-up

The experiments reported here were carried out in a recirculating wind tunnel of the Laboratoire de Mécanique des Fluides et d'Acoustique at the Ecole Centrale de Lyon. The test section of the wind tunnel was 8 m long, 1m high and 0.7 m wide. The experimental set-up was conceived in order to study flow and dispersion within a two-dimensional canyon overlain by a fully developed neutral atmospheric boundary layer, whose depth $\delta = 0.6$ m measures ten times the canyon height $H = 0.06$ m ($W = H$). This was obtained by combining three spires (Irwin, 1981) placed at the upstream end of the test section with a series of regularly spaced bars placed on the floor of the wind tunnel, normal to the wind direction. An overview of the experimental set-up is shown in Fig. 1 and fully described in previous work by Salizzoni et al. (2008, 2009).

The velocity field that develops above the obstacles is similar to an atmospheric boundary layer in neutral condition (Salizzoni et al., 2008). In the lower part of the external flow, the mean velocity profile can therefore be approximated by a logarithmic profile

$$\overline{u}(z) = \frac{u_*}{\kappa}\ln\frac{(z-d)}{z_0} \tag{5}$$

where z_0 is the roughness length, u_* is the friction velocity, d is the displacement height and κ is the von Kármán constant. According to similarity theory, the adoption of Equation (5) implies that the

[1] It is worth noting that the evaluation of $\triangle U$ at the top of the canyon is not simple as it is in the case of a canonical shear layer between two parallel flows. The definition of a criterion for the estimation of $\triangle U$ is discussed in Section 4.1.

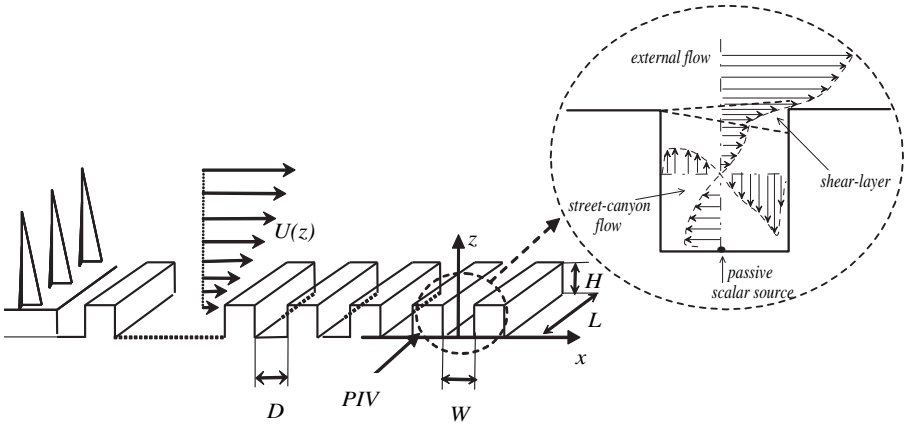

Fig. 1. Overview of the wind tunnel installation and sketch of the flow within and above the canyon within which measurements were performed.

flow is homogeneous in the horizontal plane, except below the blending height z_* in the roughness sub-layer (RSL), and that u_*, z_0, d and z_* fully characterise the different incoming wind profiles. The method adopted to evaluate these parameters is described in detail in previous studies (Salizzoni et al., 2008, 2009). In order to vary these parameters, we changed the spacing D between the upwind obstacles whilst keeping the width W of the canyon within which the transfer velocity was estimated unaltered (Fig. 1). This allowed us to obtain different incoming wind profiles characterised by different friction velocities, roughness lengths and displacement and blending heights. Four different cases have been studied and are referred to herein as configurations A, B, C and D. External flow parameters for the four configurations are given in Table 1.

We expect the integral length scale L_e to vary only with the vertical coordinate z within the core of the turbulent boundary layer flow and only to be sensitive to the obstacle spacing below the blending height z_*. From the computation of two-point spatial correlations from PIV measurements (Salizzoni, 2006) it can be inferred that in the RSL and at a given distance from the top of the obstacles, L_e increases with the width of the RSL for decreasing canyon aspect ratios H/D. An indirect proof of this was obtained by numerical simulations of the dispersion of a passive scalar (Salizzoni et al., 2009), where a turbulent diffusion coefficient K_m was modelled as the product of u_* and L_e, which was assumed constant and equal to $(z_* - H)$ over the whole of the RSL. A precise estimate of L_e would be quite difficult to achieve. The salient point here is that both L_e and u_* increase with decreasing aspect ratio H/D.

3.2. Measurement techniques

The external velocity field was measured with a hot-wire anemometer. For details refer to Salizzoni et al. (2008).

Velocities within the cavity were measured using Particle Image Velocimetry (PIV). Two coupled YAG laser sources provided pairs of laser pulses at a frequency of 4 Hz. The visualization light sheet was perpendicular to the canyon axis and measured 1 mm in width and the flow was seeded with micron-sized droplets produced by a smog generator. The observation field measured approximately 120 × 120 mm, and this was filmed at a resolution of 1280 × 1024 pixels. The interrogation window was fixed at 16 × 16 pixels, corresponding to an averaging area of 0.9 mm × 0.9 mm. The interrogation areas overlapped by 50% so that in total, each velocity field computation yielded a set of 240 × 240 vectors. In each configuration the velocity field was sampled 1000 times with a frequency of 4 Hz and these velocity fields were used to compute ensemble averaged statistics.

Ethane, chose as a passive scalar, was injected from a two-dimensional ground level source placed at the centre of the canyon. The source was constructed from a 4 cm diameter porous polymeric tube, located in a slot cut into the floor (see Fig. 2) and flush with the floor of the tunnel,[2] so as not to perturb the turbulent field within the canyon. Concentrations were measured using a Flame Ionisation Detector (FID) system with a sampling frequency of 300 Hz (Fackrell, 1980). The mass flux at the source was $M = 8.43$ mg s^{-1}, giving a mass flow rate per unit length M_q of 12 mg s^{-1} m^{-1}. The fluctuations in the mass flow rate were less than 1% (Salizzoni et al., 2009).

Table 1
External boundary layer flow parameters. $U_\infty = 6.75$ m s^{-1}, $\delta = 0.6$m and $H = 60$ mm in all four configurations.

Configuration	H/W	H/D	u_*(m s^{-1})	z_0 (mm)	d (mm)	z_*/H (−)
A	1	1	0.33	0.3	57	7/6
B	1	2/3	0.36	0.6	55	8/6
C	1	1/2	0.41	1.7	52	2
D	1	1/3	0.46	2.7	46	2

4. Experimental results

4.1. Velocity measurements

A detailed analysis of the influence of the external flow conditions on the dynamics of the flow within the cavity is provided by Salizzoni (2006) and Salizzoni et al. (submitted for publication). In the present work we restrict ourselves to the main features of the velocity field that we need to interpret the passive scalar concentration measurements presented in Section 4.

Focusing on the region at the top of the cavity ($z/H = 1$), in Fig. 3 we plot the vertical profiles of non-dimensional mean and fluctuating velocities for increasing distances from the upwind corner ($x/H = -1/3$, $x/H = 0$, $x/H = 1/3$). In Fig. 3-a–c is plotted the horizontal mean velocity $U(z)$ and in Fig. 3-a'–c' the turbulent kinetic energy (t.k.e) $\frac{1}{2}q^2(z) = \frac{1}{2}[\sigma_u^2(z) + \sigma_w^2(z)]$, where σ_u^2 and σ_w^2 are the variances of the horizontal and the vertical velocity. As the profiles in Fig. 3-a–c show, this is a region of high shear where the horizontal mean velocity rapidly drops approaching the top of the canyon from above. Similarly, the t.k.e. values change rapidly with height passing from values between 0.16 (Configuration D) and 0.08

[2] Meroney et al. (1996) provide a summary of devices that can be used to simulate ground level emissions.

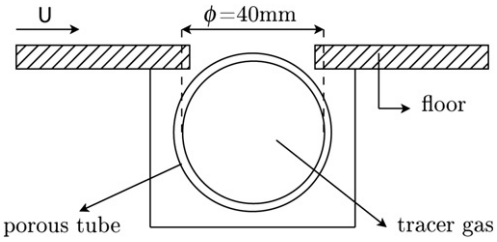

Fig. 2. Ground level source placed at the centre of the canyon.

(Configuration A) in the external flow to values that are approximately one order magnitude lower within the cavity. These differences take place over a vertical distance $l \simeq 0.2H$, which corresponds to the shear layer depth (Fig. 3).

In some aspects, the flow field at the top of the cavity is similar to the 'canonical' shear layer which develops between two laminar parallel flows with velocities U_1 and U_2, respectively, but there are distinctions:

- the flow in the cavity is not always parallel to the external flow;
- the external flow is not uniform (the mean velocities vary with the vertical coordinate);
- the turbulence kinetic energy in the external flow is not negligible $0.08 < \frac{1}{2}[q^2(z)/U_\infty^2] < 0.16$.

In the canonical case, the shear mixing layer boundaries, referred to here as z_1 and z_2, can be easily evaluated, and it is generally assumed that $\overline{u}(z_1) = 0.98U_1$, for the upper limit, and $\overline{u}(z_2) = 1.02U_2$ for the lower limit. In our case the external flow is not uniform and the boundary layer height of the external flow is much greater than the canyon height ($\delta \sim 10H$). This implies that the external velocity U_1 is not even approximately equal to U_∞ and the mean horizontal internal velocity U_2 varies with horizontal distance x, so the definition of an equivalent shear layer is rather difficult. In accordance with the analysis developed by Salizzoni (2006) and Salizzoni et al. (submitted for publication) the boundaries of the shear layer can be defined by an analysis of the profiles of t.k.e. production, $P = -\overline{u_i u_j}\frac{\partial \overline{u}_i}{\partial x_j}$. We assumed a limiting value of the derivative $\partial P/\partial z$ in order to determine the upper and lower

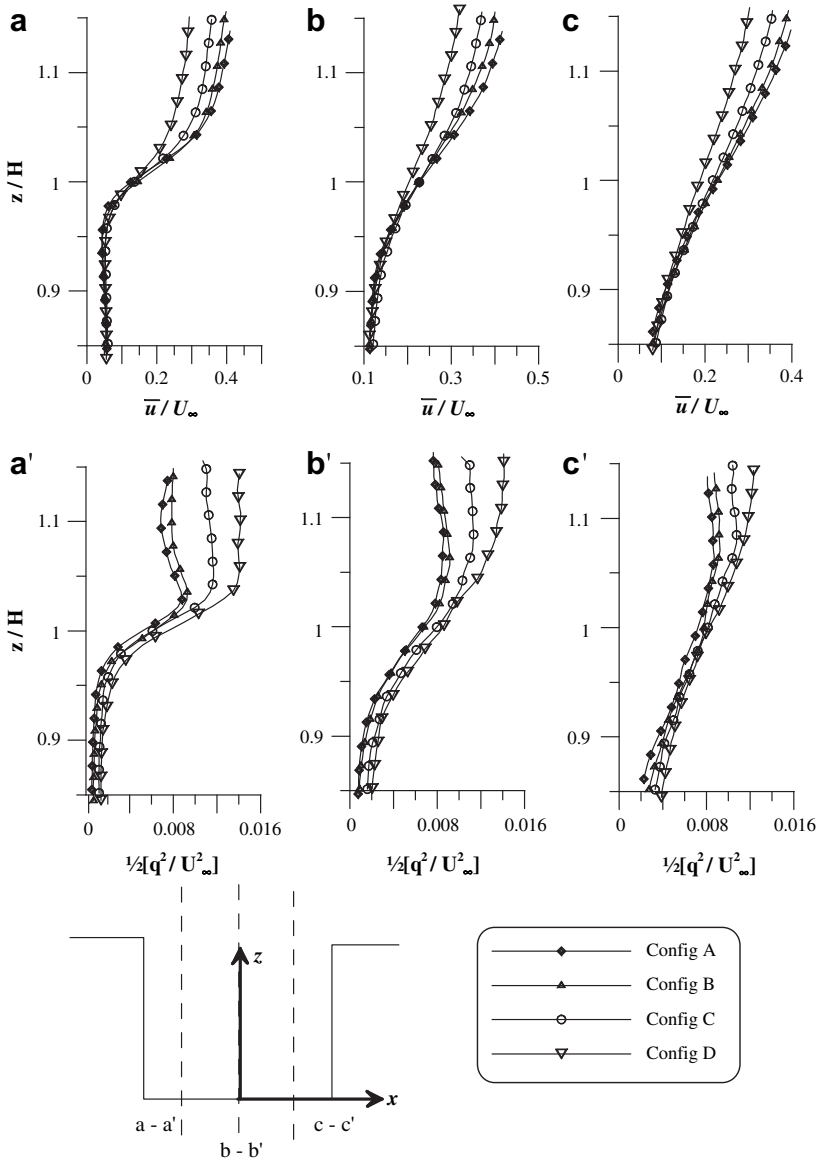

Fig. 3. Vertical profiles of normalised mean horizontal velocity and turbulent kinetic energy at the top of the cavity. Profiles are taken at $x/H = -1/3$ (a − a′), $x/H = 0$ (b − b′) and $x/H = 1/3$ (c − c′).

Table 2
Shear layer flow parameters.

Configuration	U_1 (m s^{-1})	U_2 (m s^{-1})	$\triangle U$ (m s^{-1})
A	2.88	0.743	2.13
B	2.8	0.78	2.02
C	2.5	0.83	1.67
D	2.15	0.73	1.42

boundary between the region where it varies relatively rapidly within the shear layer and the region where it attaints a constant value outside. The values of $\triangle U$ for the four configurations are given in Table 2. The criterion adopted to compute $\triangle U$ is somewhat arbitrary and it could be replaced by another that would lead to different values. However, whatever the criterion is, from the profiles plotted in Fig. 3-a–c, it is clear that the value of $\triangle U$ has to increase from Configuration A to Configuration D, and therefore for decreasing values of the aspect ratio of the upwind canyons H/D.

Within the cavity the mean flow is characterised by the presence of a principal recirculating cell, with smaller counter-rotating vortices in the corners, as shown by the streamlines plotted in Fig. 4-a. It is worth noting that the t.k.e. levels within the cavity are about one order of magnitude lower than those in the external flow (Fig. 4-b). Furthermore, the t.k.e. values within the canyon are quite uniform except close to the downwind wall. There, a t.k.e. plume extends down into the canyon from the upper edge along the downwind wall.

If we compare the velocity profiles obtained for the four different configurations (Fig. 5), we observe that the mean and fluctuating flows within the cavity exhibit significantly different dependencies on the dynamical condition of the external flow. In fact, while the mean velocities appear to be quite insensitive to the difference in the external flow conditions (Fig. 5-a), the horizontal (Fig. 5-b) and vertical (Fig. 5-c) profiles of the t.k.e. show important differences from one configuration to the other. The results show that the intensity of the t.k.e. field of the external flow is reflected within the cavity, and that increased external turbulence levels, which we measure by the ratio u_*/U_∞ given in Table 1, induce an increased intensity of the fluctuating flow within the canyon.

4.2. Passive scalar concentration measurements

To study the dispersion of a passive scalar emitted by a line source at ground level we performed two kinds of experiments, in steady and in unsteady conditions.

4.2.1. Steady experiments: mean concentration field

In steady state conditions, the mean concentrations within the cavity were measured on a regularly spaced grid. Mean concentration fields were then obtained for each configuration by interpolating between the experimental points. An example is given in Fig. 6, where the mean concentration field for Configuration A is plotted. The concentration fields in the four configurations are similar to those obtained in similar experiments (Kastner-Klein and Plate, 1999; Soulhac et al., 2001), showing quite uniform values within the cavity except close to the source and to the walls. Higher concentrations are detected close to the upwind wall whereas lower concentrations are detected close to the downwind wall, where the inflow of fresh air from the external flow dilutes the passive scalar. Since the concentration fields are similar to each other, the time-averaged concentration can be described as:

$$C(x,\ z) = < C > g(x,\ z)$$

where $< C >$ is the spatially averaged concentration and $g(x, z)$ is a form function (Soulhac, 2000). An estimation of $< C >$ for the four configurations obtained by averaging the measures over a regular grid (Fig. 6) are given in Table 3. The results show that the spatially averaged concentration within the canyon decreases from Configuration A to Configuration D, i.e. for increasing values u_*. The concentrations in Table 3 and in Fig. 6 are shown expressly in dimensional form, since their normalisation would require a reference velocity, which is in fact the final aim of this study.

4.2.2. Unsteady experiments: measurement of the canyon wash-out curves

Another series of experiments was performed in unsteady conditions in order to measure the wash-out time of the cavity and hence a typical mass-transfer velocity. In order to estimate the exchange velocity experimentally, several approaches can be adopted. Some authors (Caton et al., 2003; Dezso-Weidinger et al., 2003) have measured the spatially averaged concentration within the cavity as it empties using a Particle Tracking Velocimetry technique. Others evaluated the sublimation time of naphthalene (Barlow and Belcher, 2002; Barlow et al., 2004) or water (Narita, 2007) from the canyon facets.

We have estimated the mass exchange between the canyon and the external flow by measuring the time for the pollutant to be washed out of the cavity at a fixed point. Ethane was injected into the canyon until the concentration field reached a stationary state. The injection of ethane was halted by means of valves placed at the extremities of the tube and the temporal evolution of its

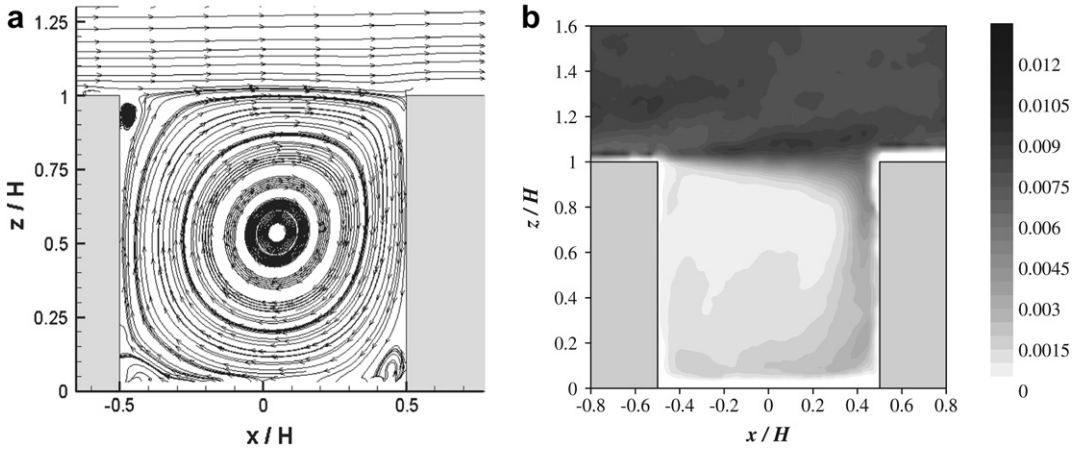

Fig. 4. Velocity field (PIV measurement) within the canyon for Configuration A. a) Mean flow streamlines; b) normalised turbulent kinetic energy $\frac{1}{2}[q^2(z)/U_\infty^2]$.

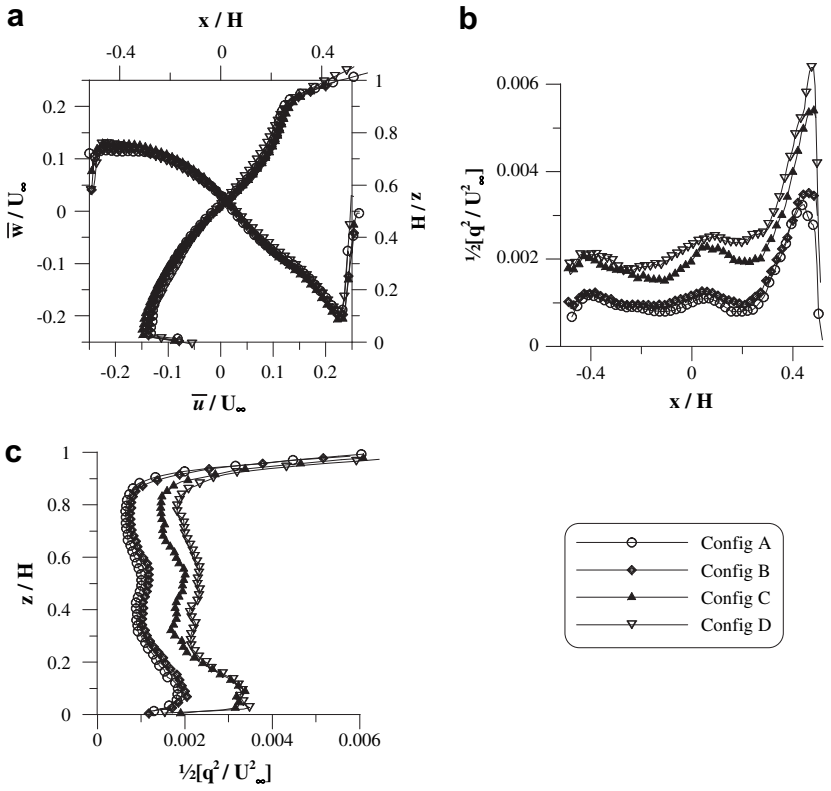

Fig. 5. Velocity profiles within the cavity. a) Vertical profile at $x/H = 0$ of the mean velocity $\overline{u}$ and horizontal profile at $z/H = 1/2$ of the mean vertical velocity $\overline{w}$; b) horizontal profile of t.k.e. at $z/H = 0.5$; c) vertical profile of t.k.e. at $x/H = 0$.

concentration $\widehat{c}(t)$ within the cavity recorded as it emptied (Fig. 7). The experiments were performed by placing the FID probe in different positions within the cavity. At each measurement point, the experiment was repeated 50 times to allow an ensemble average $\widehat{C}(t)$ of the signals to be computed (Fig. 7). For Configuration A, we registered 1000 signals to obtain an estimate of the experimental error (Section 6).

Fig. 7-a shows that the concentration signals asymptotically approach a non-zero value (here $\widehat{C} \simeq \widehat{C}_b$ for $t \simeq 10$ s). This background concentration, $\widehat{C}_b$, has two different sources. Firstly, the experiments were performed in a recirculating wind tunnel and therefore the passive scalar accumulated within it. Secondly, since the valves were placed at the extremities of the porous tube, air containing a high concentration of the passive scalar was trapped within the tube even after the injection was stopped, i.e. for $t > 0$ (Fig. 7-a). The source therefore continued to emit a small pollutant flux driven by the pressure differences between the interior of the porus tube and the exterior environment (caused by the turbulent velocity fluctuations within the cavity). The background concentration $\widehat{C}_b$ was calculated for each series of experiments and subtracted from the averaged wash-out curves so that the normalised concentrations $C/C_0 = [\widehat{C}(t) - \widehat{C}_b]/[\widehat{C}(0) - \widehat{C}_b]$ asymptotically approached zero, as shown in Fig. 7-b.

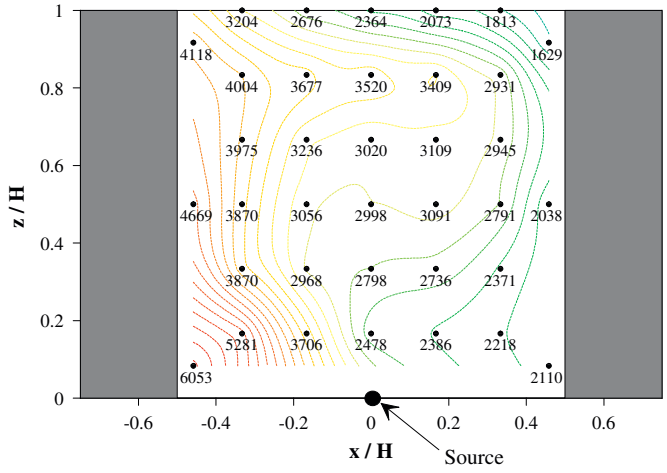

Fig. 6. Mean concentration(mg m^{-3}) field within the cavity for Configuration A; $U_\infty = 6.75$ m s^{-1}, $H = 60$ mm, $u_* = 0.33$ m s^{-1}, $\dot{M}_q$ of 12 mg s^{-1} m^{-1}.

Measurements were taken for each of the external flow configurations at five different points within the cavity (Fig. 8). One point was located at the canyon centre ($x/H = 0, z/H = 1/2$ – point a) whilst the others were located at a radial distance of $H/3$ from the centre. Fig. 8 shows the wash-out curves that we measured at different position within the canyon for Configuration A.

The results show that all curves have a horizontal tangent for $t \to 0$ which indicates an 'initial delay' in the wash-out process. A similar trend can be observed in the wash-out curve measured by Caton et al. (2003) in a square cavity and by Mavroidis et al. (1999) in the wake of an obstacle. However, in their case the curve refers to a concentration spatially averaged over the whole canyon. The initial delay is particularly evident for the curves registered at the centre of the canyon ($z = H/2$ and $x = 0$), which differ significantly

Table 3
Spatially averaged concentration $< C >$ (mg m^{-3}) within the canyon.

Configuration	A	B	C	D
$< C >$	3100	2864	2732	2635

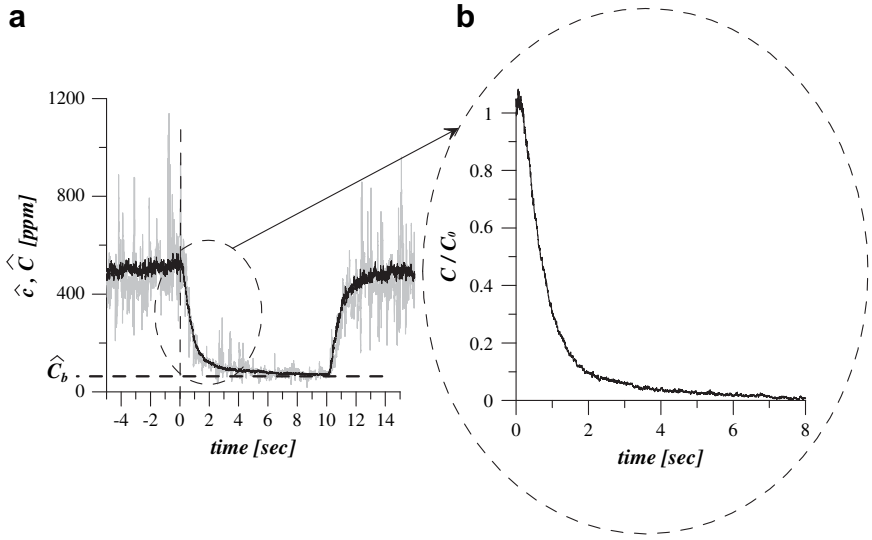

Fig. 7. Wash-out concentration measurements in function of time. a) Grey line: single signal $\hat{c}(t)$; black line: curve averaged over 50 signals $\hat{C}(t)$. b) Dimensionless wash-out curve obtained by subtracting the background concentration $\hat{C}_b$.

from those measured towards the perimeter. The trend of the curves measured at the other four positions, outside of the canyon core, are very similar to each other. The only difference can be observed in curve d), measured near the downwind wall, which is characterised by higher fluctuations of the ensemble averaged curve. This is probably due to the enhanced velocity fluctuations, as we observed in the t.k.e. field (Fig. 4-b), which induce higher fluctuations of the passive scalar concentrations. Otherwise, curve d) does not differ significantly from curves b), c) and e). This means that the characteristic 'turn-over' velocity scale is far larger than a 'diffusive' velocity scale within the canyon. It is worth noting that this result implies that advection due to the mean velocity does not play any role in the wash-out process, which is instead completely controlled by the fluctuating component of the velocity field.

Since the curves registered at the equal radial distance from the centre do not differ (curves b–e in Fig. 8), we only recorded the wash-out curves at two different locations: the cavity centre ($x/H = 0$, $z/H = 1/2$) and close to the upwind wall ($x/H = -1/3$, $z/H = 1/2$). A comparison between the results obtained in the four different configurations (Fig. 9) shows that the normalised concentrations decrease more rapidly as a function of time for increasing u_*. As u_* increases, from Configuration A to D (see Table 1), both the external velocity U_1 and the velocity difference across the shear layer ΔU decrease (see Table 2). It is then clear that α (Equation (3)) cannot be a constant. This result demontrates experimentally that the transfer velocity is influenced by the structure of the atmospheric turbulence and that α must be a function of $u_*/\Delta U$ and L_e/H.

We developed an analytical model to interpret the wash-out curves. By comparing analytical predictions and experimental results we may then quantify the transfer velocity and its dependence on the dynamical condition of the external flow.

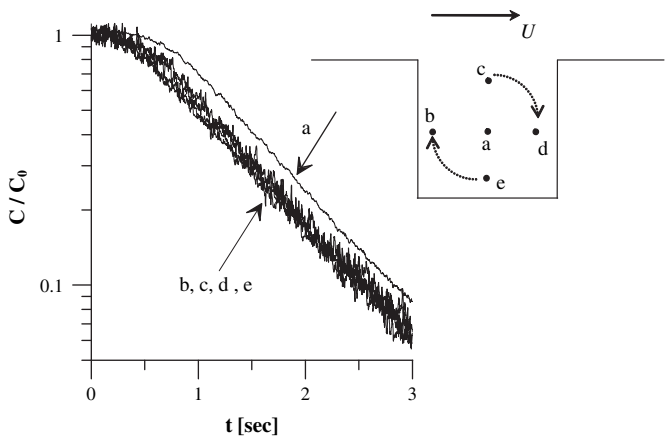

Fig. 8. Wash-out curves measured at different position within the cavity for Configuration A.

5. Modelling

As we have seen in Section 4, the wash-out curves show two main features:

- a horizontal tangent for $t \to 0$;
- the normalised concentrations measured at the cavity centre differs from those measured towards the cavity perimeter.

The horizontal tangent, which is due to an initial mixing process acting on the non-uniform concentrations within the canyon, suggests that more than one time scale is involved in the wash-out process. For this reason the adoption of a box model with one degree of freedom leading to an exponential decay with a negative tangent for $t \to 0$ is inappropriate. Therefore, we have developed a model with two degrees of freedom. We assume that the flow is made up of three different regions as shown in Fig. 10, each containing a uniform concentration of pollutant. One box represents the external flow while the other two give a rough description of the pollutant distribution inside the canyon. Box 2 represents the core of the flow inside the cavity, while box 1 represents the recirculating part of the flow, which leads pollutant towards the shear layer at the top of the cavity.

The mass transport can now be described by means of a sequence of transfers between these three regions. A mass balance for the two boxes within the cavity yields:

$$\begin{cases} V_1 \frac{dC_1}{dt} = S_{10} u_d (C_{ext} - C_1) + S_{12} \tilde{u}_d (C_2 - C_1) + \dot{M}_q \\ V_2 \frac{dC_2}{dt} = S_{12} \tilde{u}_d (C_1 - C_2) \end{cases} \quad (6)$$

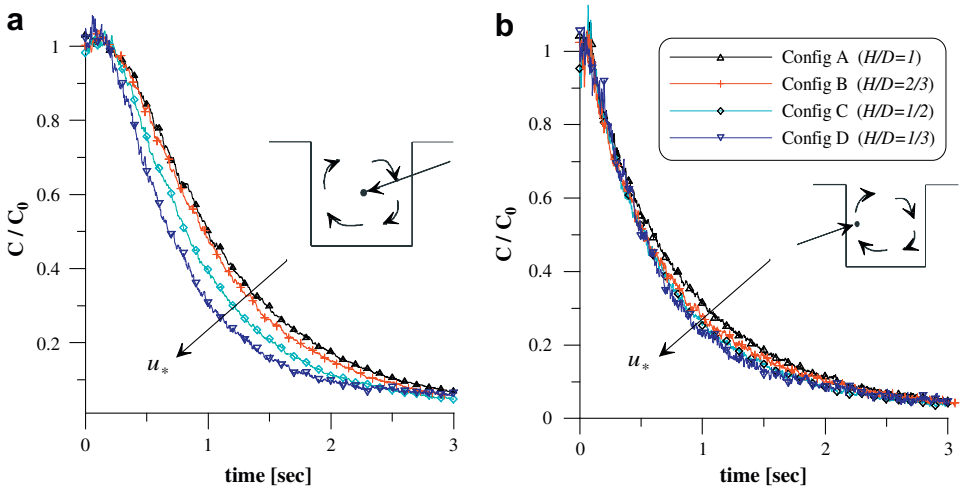

Fig. 9. Wash-out curves measured within the cavity for the four cases studied. a) Concentrations registered at the $x/H = 0$, $z/H = 1/2$; b) Concentrations registered at $x/H = -1/3$, $z/H = 1/2$.

where V_1, V_2, C_1 and C_2 are the volume per unit length (namely, an area in this two-dimensional situation) and average concentrations of, respectively. S_{10} and u_d represent the exchange surface per unit length (namely, a length in this two-dimensional situation) and transfer velocity between box 1 and the external flow whilst S_{12} and $\tilde{u}_d$ are the exchange surface (per unit length) and transfer velocity between box 2 and the box 1. S_{10} is equal to the canyon width, i.e. $S_{10} = W = H$. Conversely, S_{12} and therefore V_1 and V_2 cannot be determined *a priori* and their value is arbitrary. In order to determine the surface S_{12} we can represent the box 2 as a circle of radius $\mathcal{R}$ placed in the centre of the canyon, so that

$$S_{12} = 2\pi\mathcal{R} \tag{7}$$

and

$$V_2 = \pi\mathcal{R}^2 \tag{8}$$

Volumes V_1 and V_2 can be expressed as a function of the volume of the whole canyon $V = H^2$. We set

$$V_1 = \beta V \tag{9}$$

$$V_2 = (1-\beta)V \tag{10}$$

where the constant $0 < \beta < 1$.

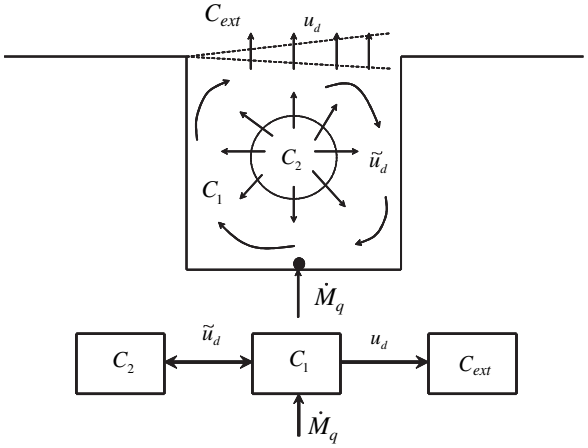

Fig. 10. Simplified model of the pollutant transfer within a square cavity with a ground level source.

By combining Equations (8)–(10) the radius $\mathcal{R}$ can be expressed as a function of β:

$$\mathcal{R} = \sqrt{\frac{1-\beta}{\pi}}H \tag{11}$$

Finally, by assuming that without loss of generality $C_{ext} = 0$ and by substituting Equations (7)–(11) into Equation (6) we obtain:

$$\begin{cases} \dfrac{dC_1}{dt} = -\dfrac{1}{\beta H}u_d C_1 + \dfrac{2\sqrt{(1-\beta)\pi}}{\beta H}\tilde{u}_d(C_2 - C_1) + \dfrac{\dot{M}_q}{\beta H^2} \\ \dfrac{dC_2}{dt} = \dfrac{2\sqrt{(1-\beta)\pi}}{(1-\beta)H}(C_1 - C_2)\tilde{u}_d \end{cases} \tag{12}$$

5.1. Steady conditions

When the system reaches a steady state, we can write

$$\begin{cases} -\dfrac{1}{\beta H}u_d C_{1ss} + \dfrac{2\sqrt{(1-\beta)\pi}}{\beta H}\tilde{u}_d(C_{2ss} - C_{1ss}) + \dfrac{\dot{M}_q}{\beta H^2} = 0 \\ \dfrac{2\sqrt{(1-\beta)\pi}}{(1-\beta)H}\tilde{u}_d(C_{1ss} - C_{2ss}) = 0 \end{cases} \tag{13}$$

and therefore

$$C_{1ss} = C_{2ss} = \frac{\dot{M}_q}{u_d H} \tag{14}$$

which indicates that, according to our model, the mean concentration in the two boxes must be equal once the steady state has been reached. Equation (14) also shows that in steady state conditions and the case of a source placed at the ground (box 1), the concentration within the boxes is imposed by the transfer velocity u_d and is independent of $\tilde{u}_d$. Equation (14) can be used in order to determine the transfer velocity u_d, using the spatially averaged concentrations within the canyon given in Table 3. The results are presented in Table 4.

Table 4
Estimation of the wash-out velocities u_d (m s^{-1}) by means of steady state concentration measurements.

Configuration	A	B	C	D
u_d	0.064	0.070	0.073	0.076

The error in the evaluation of u_d depends upon the accuracy of the estimate of the inflow mass rate $\dot{M}_q$ and of the absolute value of the spatially averaged concentration within the canyon in steady conditions. A continuous monitoring of the mass inflow rate revealed that the fluctuations of $\dot{M}_q$ were less than 1%. However, errors in the mean concentration measurements with an FID can reach 10% (Salizzoni, et al., submitted for publication). These are mainly due to errors in the evaluation of the calibration constants, which are sensitive to atmospheric pressure and temperature variations. Estimates of u_d with steady state measurement using Equation (14) are therefore subject to errors which may be greater than the differences of the values of u_d that we would expect to measure. Since these results are not reliable, we adopted another method to estimate u_d, which is not sensitive to errors in the absolute values of the mean concentrations. This method is based on the interpolation of the wash-out curves with a solution to Equation (12) in unsteady conditions, as described in the next section.

5.2. Unsteady conditions

In order to model the temporal evolution of a passive scalar concentration within the cavity as it empties we can set $\dot{M}_q = 0$ in Equation (12). The initial conditions are are provided by Equation (14) so that $C_1(0) = C_{1ss} = C_2(0) = C_{2ss}$. We can then rewrite Equation (12), in non-dimensionalised form, via a change of variables

$$C_1 = C_1' C_{1ss}$$
$$C_2 = C_2' C_{2ss}$$

thus obtaining

$$\begin{cases} \dfrac{dC_1'}{dt} = -\dfrac{1}{\beta H} u_d C_1' + \dfrac{2\sqrt{(1-\beta)\pi}}{\beta H} \tilde{u}_d (C_2' - C_1') \\ \dfrac{dC_2'}{dt} = \dfrac{2\sqrt{(1-\beta)\pi}}{(1-\beta)H} (C_1' - C_2') \tilde{u}_d \\ C_1'(0) = 1 \\ C_2'(0) = 1 \end{cases} \tag{15}$$

The system of equation (15) admits a solution of the form

$$\begin{cases} C_1' = C_1'(t; u_d, \tilde{u}_d, \beta) \\ C_2' = C_2'(t; u_d, \tilde{u}_d, \beta) \end{cases} \tag{16}$$

which is given in the Appendix. The analytical solution given by Equation (16) has therefore three free parameters: $u_d, \tilde{u}_d, \beta$. These can be used to fit the experimental curves in order to estimate the transfer velocities u_d and $\tilde{u}_d$, once the value of β has been fixed as we discuss in the next paragraph. We stress that this approach allows us to estimate the transfer velocities u_d and $\tilde{u}_d$ from the temporal evolution of the dimensionless concentrations $C'_1(t)$ and $C'_2(t)$, which are independent of calibration errors of the FID probe.

6. Comparison with experimental results and discussion

In order to estimate the transfer velocities u_d and $\tilde{u}_d$ as a function of the dynamic conditions of the external flow, equations (16) were fitted to the measured wash-out curves by adjusting the values of u_d and $\tilde{u}_d$ so as to minimize the sum of the square of the differences between the theoretical and the measured points. However, the volumes of the two boxes V_1 and V_2 must be accounted for with a parameter β which becomes a third unknown in our system. The problem can therefore be defined as follows:

$$E = \sum_{n=0}^{n=1500} \left\{ \left[C'_{\exp 1}(n) - C_1'\left(n; u_d, \tilde{u}_d, \beta\right) \right]^2 + \left[C'_{\exp 2}(n) - C_2'\left(n; u_d, \tilde{u}_d, \beta\right) \right]^2 \right\},$$

with

$$\frac{\partial E}{\partial u_d} = 0, \quad \frac{\partial E}{\partial \tilde{u}_d} = 0, \quad \frac{\partial E}{\partial \beta} = 0.$$

where $C'_{exp1}(n)$ and $C'_{exp2}(n)$ are the non-dimensional ensemble averages of the experimental concentration registered at the n-th time step (normalised by means of the steady state concentration registered at the same location). The estimate is performed for over 5 s; since the sample frequency is 300 *Hz*, the best fit is thus calculated for $0 \le n \le 1500$. Estimates performed over larger time interval do not differ significantly since both experimental and theoretical values are very close to zero for $t > 5$ s. The inclusion of β as an unknown makes the problem non-linear, so that it is not possible to obtain an analytical solution for the 3 unknown parameters that will minimize the total error. However, if β is known, an analytical solution is readily obtained for u_d and $\tilde{u}_d$. The parameters were determined by assuming different values for β within a predetermined range ($\beta = 0.8$, 0.85 and 0.9) and solving analytically for u_d and $\tilde{u}_d$. The values of β correspond to circles whose radii are $\mathcal{R} = 0.25H$, $0.22H$ and $0.18H$ respectively. These radii have been determined via an analysis of Fig. 6, estimating the area of the region at the core of the canyon where the passive scalar concentration is approximately uniform. Results for the transfer velocities u_d and $\tilde{u}_d$ are given in Table 5 for corresponding values of β, together with the dependence of the total error E on the assumed value of β. Table 5 shows the values of the typical wash-out times of the two boxes T_1 and T_2 defined as

$$T_1 = \frac{\beta V}{S_{10} u_d} = \frac{\beta H}{u_d} \quad \text{and} \quad T_2 = \frac{(1-\beta)V}{S_{21}\tilde{u}_d} = \sqrt{\frac{(1-\beta)}{\pi}} \frac{H}{\tilde{u}_d}$$

The error E in configurations A, B and C are similar whilst the error in Configuration D is almost double that in the other cases.

Table 5
Variation of the wash-out time and of the exchange velocities as a function of the turbulence intensity of the external flow. $\tilde{u}_d$ and u_d are in m s^{-1}, T_1 and T_2 are in seconds, E is dimensionless. $H = 60$ mm, $U_\infty = 6.75$ m s^{-1}.

Configuration		$\beta = 0.8$	$\beta = 0.85$	$\beta = 0.9$
A	u_d	0.066 ± 0.0026	0.066 ± 0.0026	0.066 ± 0.0026
	T_1	0.72	0.77	0.81
	$\tilde{u}_d$	0.019 ± 0.0011	0.017 ± 0.001	0.014 ± 0.0008
	T_2	0.39	0.39	0.39
	E	6.06	5.42	4.99
B	u_d	0.073 ± 0.0029	0.073 ± 0.0026	0.074 ± 0.0026
	T_1	0.66	0.69	0.73
	$\tilde{u}_d$	0.021 ± 0.0012	0.018 ± 0.0011	0.016 ± 0.0009
	T_2	0.32	0.36	0.40
	E	5.27	4.85	4.76
C	u_d	0.076 ± 0.0030	0.076 ± 0.0031	0.077 ± 0.0031
	T_1	0.63	0.66	0.70
	$\tilde{u}_d$	0.026 ± 0.0015	0.022 ± 0.0013	0.018 ± 0.0011
	T_2	0.29	0.29	0.29
	E	7.27	6.77	6.43
D	u_d	0.078 ± 0.0031	0.079 ± 0.0031	0.079 ± 0.0031
	T_1	0.61	0.65	0.68
	$\tilde{u}_d$	0.041 ± 0.0024	0.035 ± 0.0021	0.030 ± 0.0017
	T_2	0.14	0.18	0.18
	E	12.53	12.16	11.84

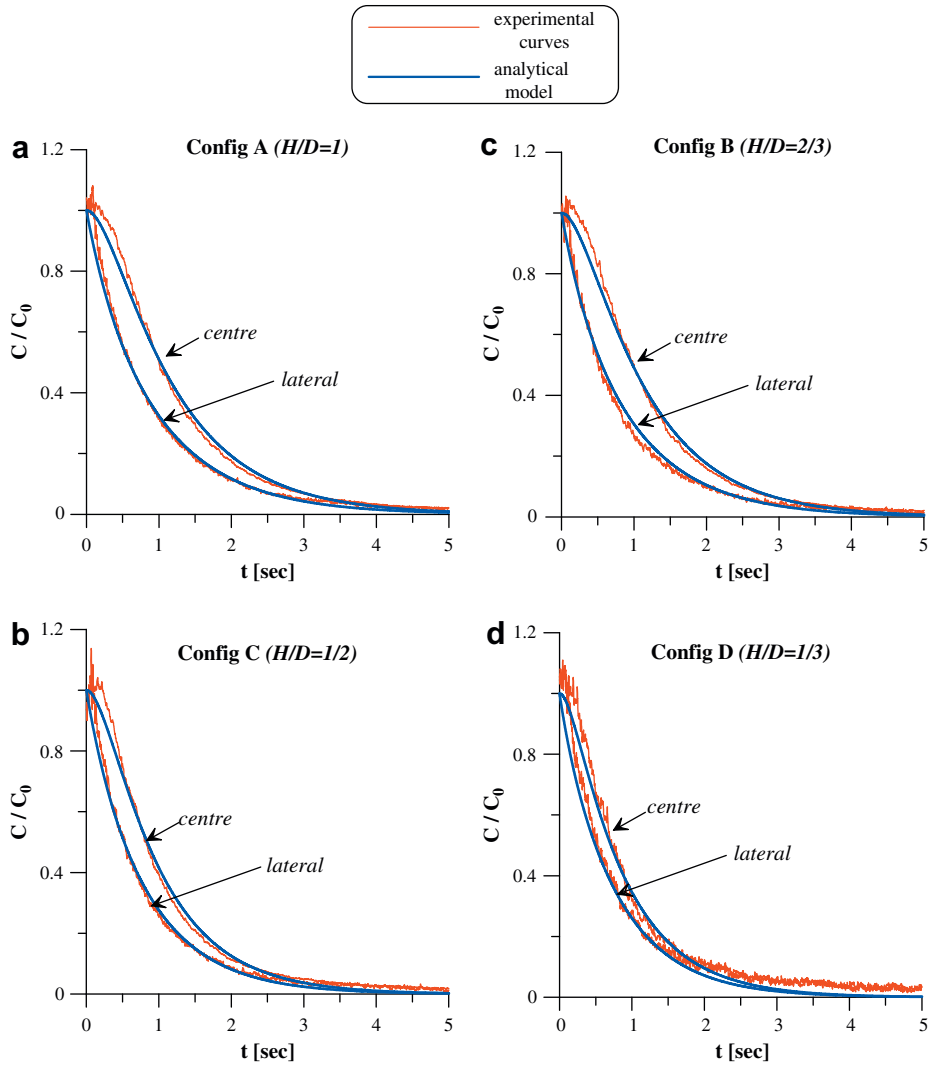

Fig. 11. Comparison between experimental results and analytical model obtained by fitting Equation (16) to the experimental results with $\beta = 0.85$; 'centre' refers to point a) in Fig. 8, 'lateral' refers to point b) in Fig. 8.

Table 5 shows that the estimates of u_d are relatively insensitive to the chosen value of the arbitrary constant β, unlike $\tilde{u}_d$ which exhibits a non-negligible dependency.

The experimental errors in the estimate of the wash-out velocities have been computed from 20 different estimates of u_d and $\tilde{u}_d$ obtained from 20 sets of 50 wash-out curves registered for configuration A. This analysis was performed only for Configuration A and we have assumed that wash-out velocities in the four different configurations have the same relative error. From the 1000 signals we obtained 20 different ensemble averaged curves (both for the centre of the cavity, i.e. point a) in Fig. 8, and for the lateral, i.e. point b) in Fig. 8) and therefore 20 different estimates of the wash-out velocities u_d. Once computed, the standard deviation σ_{ud} and the mean $<$ ud $>$ of these 20 values of u_d gave the relative experimental error $e = \sigma_{u_d}/< u_d >$. We found this relative error to be $e = 4\%$ for u_d and $e = 6\%$ for $\tilde{u}_d$.

The velocity u_d is generally two or three times larger than $\tilde{u}_d$. This can be explained by the presence of the high t.k.e. plume close to the downwind wall (Fig. 4) which certainly enhances the mass transfer within the box 1, the outer box, compared to that in the box 2, the central box (Fig. 10).

A comparison between experimental and theoretical curves for the four configurations is shown in Fig. 11. The analytical solutions follow satisfactorily the experimental curves, both at the centre of the cavity, i.e. point a) in Fig. 8, and close to the upwind wall, i.e. point b) in Fig. 8. In particular, the model reproduces the horizontal tangent of the wash-out curves registered at the cavity centre. This result confirms that the simplified description of mass transfer given by the two-box model (and sketched in Fig. 10) gives a satisfactory description of the transport of pollutant from the cavity towards the external flow.

6.1. Characteristic velocity, length and time scales

We can identify three different transfer processes characterised by different velocity scales and lengths:

- turbulent dispersion within the canyon whose velocity scale is related to the square root of the approximately constant t.k.e. within the canyon away from the downwind wall (Fig. 4). The length scale is the canyon height H.
- advection due to the mean recirculating flow. The velocity scale can be reasonably assumed asU_2, i.e. the mean horizontal internal velocity at the lower boundary of the shear layer. The length scale is the canyon height H.

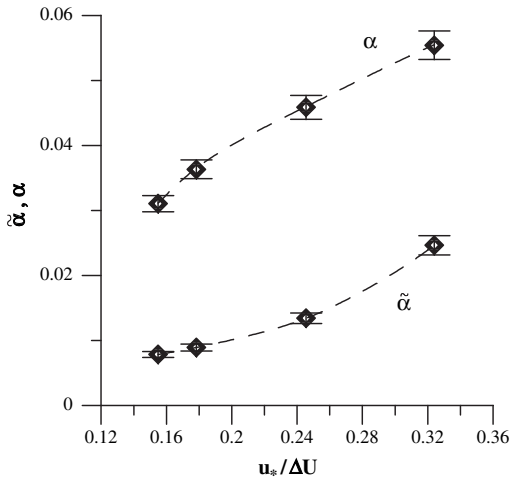

Fig. 12. Dependence of α and $\tilde{\alpha}$ on the turbulence intensity of the external flow ($\beta = 0.85$); the error bars are calculated over 20 estimates of u_d and $\tilde{u}_d$ (Table 5).

- turbulent dispersion across the shear layer, whose characteristic velocity must scale with $\triangle U$, the mean velocity difference across the shear layer and whose characteristic length scale is the shear layer depth $l \sim 0.2H$ (Fig. 3).

We can therefore define three time scales associated with each process and evaluate them assuming typical values for Configuration A:

- a time scale of the turbulent dispersion within the canyon $\tau_1 \sim \frac{H}{\sqrt{q^2/2}} \sim \frac{0.06}{0.2} \sim 3{\cdot}10^{-1}$ seconds;
- a time scale related to the mean recirculating motion $\tau_2 \sim \frac{H}{U_2} \sim \frac{0.06}{1} \sim 6{\cdot}10^{-2}$s;
- a time scale related to the transfer across the shear layer $\tau_3 \sim \frac{l}{\Delta U} \sim \frac{0.012}{2} \sim 6{\cdot}10^{-3}$ s.

The three time scales cover three orders of magnitude. By looking at the computed time scales T_1 and T_2 in Table 5 we see that these are of the same order of magnitude as τ_1 and are much larger that the two other scales τ_2 and τ_3. Observing the process with a typical wash–out scale (T_1 or T_2) suggests that once a pollutant particle reaches the shear layer it is 'instantaneously' transferred out of the canyon. Similarly, the typical turn-over time of a particle due to the mean recirculating motion is much smaller that the wash-out time, which means that the turn-over velocities far exceeds the typical wash-out velocity. This feature is consistent with the wash-out curves presented in Fig. 8, where it is evident that the wash-out process has to be independent of the mean recirculating motion within the cavity. Following Harman et al. (2004) and Yang and Shao (2006) we can draw an electrical analogy and describe the transfer process as akin to resistances in series, related to the three transfer mechanisms outlined. As with an electrical circuit, the transfer is governed by the process that creates the highest resistance. In this case, the wash-out process is regulated by the lowest transfer, related to the fluctuating component of the velocity field, which imposes its typical time and velocity scales on the whole process.

6.2. Influence of the atmospheric turbulence

A principal aim of this study was to define how sensitive the mass-transfer velocity was to the external flow conditions and compare our results with the assumptions presented in Section 2. Our experimental results clearly show that α is a function of the dynamical conditions of the external flow,

$$\frac{u_d}{\Delta U} = \alpha\left(\frac{u_*}{\Delta U}; \frac{L_e}{H}\right)$$

The same result holds for $\tilde{u}_d$ and the corresponding function $\tilde{\alpha}$,

$$\frac{\tilde{u}_d}{\Delta U} = \tilde{\alpha}\left(\frac{u_*}{\Delta U}; \frac{L_e}{H}\right)$$

The functions α and $\tilde{\alpha}$ are plotted in Fig. 12 against the values of $\frac{u_*}{\Delta U}$ in the four configurations studied. It is worth noting that the experimental results do not allow us to define separately the influence of $\frac{u_*}{\Delta U}$ and $\frac{L_e}{H}$ on α and $\tilde{\alpha}$ since these two parameters both vary in the four configurations. However, α and $\tilde{\alpha}$ increase when both parameters are increased.

The dependence of α and $\tilde{\alpha}$ on the structure of the external flow indicates that the transfer process is not only due to turbulent structures generated locally within the shear layer or canyon. In fact, the non-linear interaction of locally generated vortices with vortices travelling in the external flow plays a major role in this transfer process. The flapping motion of the shear layer induces the coupling of locally generated vortices with those travelling in the external flow. These are grasped and drawn into the canyon at the downwind corner. This intermittent entrainment of vortical structures drives the entire transfer process.

7. Conclusions

We have studied the mass exchange between a street canyon and the external atmospheric flow by means of wind tunnel experiments. Velocity and passive tracer concentration fields were measured within a square canyon overlain by a simulated neutral atmospheric boundary layer. The mass-transfer velocity was estimated by measuring the time evolution of the tracer concentration within the cavity as it emptied. The experimental results have been interpreted by means of the analytical solution of a system of two differential equations, obtained by modelling the mass transfer within the cavity with a two-box model. The good agreement between experimental and theoretical results has allowed us to clarify the basic mechanisms that drive the mass transfer. This appears to be entirely governed by the fluctuating component of the turbulent flow and not affected by the magnitude of the mean recirculating flow within the canyon.

In order to define the dependence of the turbulent mass transfer on the structure of the external flow, we performed the experiments for varying dynamical conditions of the external flow. Velocity measurements show that the intensity of the fluctuating flow within the cavity depends on the intensity of the external turbulence. Similarly passive scalar dispersion results show that the transfer velocity is also enhanced for increasing intensity of the external turbulence. This feature demonstrates conclusively that the external turbulence has a direct influence on the flow and dispersion within the canyon and hence on the whole turbulence transfer between the canyon and the atmosphere.

Acknowledgments

The authors would like to express their gratitude to A. Ezzamel and G.R. Hunt for carefully reading the paper and providing a critical review of its content.

Appendix 1

We define

$$\mathcal{A} = -\frac{u_d}{\beta H}$$

$$\mathcal{D} = \frac{2\sqrt{(1-\beta)\pi}}{H}\tilde{u}_d$$

and rewrite the system of equations (15) as

$$\begin{cases} \dfrac{dC_1'}{dt} = \mathcal{A}C_1' + \dfrac{\mathcal{D}}{\beta}(C_2' - C_1') \\ \dfrac{dC_2'}{dt} = \dfrac{\mathcal{D}}{(1-\beta)}(C_1' - C_2') \\ C_1'(0) = 1 \\ C_2'(0) = 1 \end{cases} \tag{17}$$

The system of equations (17) admits the following solution

$$C_1'(t) = \left[\frac{\mathcal{D}+\Gamma-\mathcal{A}\beta^2+\mathcal{A}\beta}{2\Gamma}\exp\left\{\frac{t\left(\mathcal{D}-\Gamma+\mathcal{A}\beta^2-\mathcal{A}\beta\right)}{2\beta^2-2\beta}\right\} + -\frac{\mathcal{D}-\Gamma-\mathcal{A}\beta^2+\mathcal{A}\beta}{2\Gamma}\exp\left\{\frac{t\left(\Gamma+\mathcal{D}+\mathcal{A}\beta^2-\mathcal{A}\beta\right)}{2\beta^2-2\beta}\right\}\right]$$

$$C_2'(t) = \left[\left(\Gamma-\mathcal{A}\beta-2\mathcal{D}\beta+\mathcal{A}\beta^2+\mathcal{D}\right)\left(\frac{\mathcal{D}+\Gamma-\mathcal{A}\beta^2+\mathcal{A}\beta}{2\Gamma}\right) \times\exp\left\{\frac{t\left(\mathcal{D}-\Gamma+\mathcal{A}\beta^2-\mathcal{A}\beta\right)}{2\beta^2-2\beta}\right\}+\left(\Gamma+\mathcal{A}\beta+2\mathcal{D}\beta-\mathcal{A}\beta^2-\mathcal{D}\right) \times\left(\frac{\mathcal{D}-\Gamma-\mathcal{A}\beta^2+\mathcal{A}\beta}{2\Gamma}\right)\exp\left\{\frac{t\left(\Gamma+\mathcal{D}+\mathcal{A}\beta^2-\mathcal{A}\beta\right)}{2\beta^2-2\beta}\right\}\right] \Big/ [2D(1-\beta)]$$

where

$$\Gamma = \sqrt{A^2\beta^4 - 2A^2\beta^3 + A^2\beta^2 - 4\mathcal{A}\mathcal{D}\beta^3 + 6\mathcal{A}\mathcal{D}\beta^2 - 2\mathcal{A}\mathcal{D}\beta + \mathcal{D}^2}$$

References

Barlow, J.F., Belcher, S.E., 2002. A wind tunnel model for quantifying fluxes in the urban boundary layer. Boundary-Layer Meteorology 104, 131–150.

Barlow, J.F., Harman, I.N., Belcher, S.E., 2004. Scalar fluxes from urban street canyons. part 1: laboratory simulation. Boundary-Layer Meteorology 113, 369–385.

Berkowicz, R., Hertel, O., Larsen, S.E., Sorensen, N.N., Nielsen, M., 1997. Modelling Traffic Pollution in Streets. Tech. rep.. National Environmental Research Institute.

Cai, X.-M., Barlow, J.F., Belcher, S.E., 2008. Dispersion and transfer of passive scalars in and above street canyons – large-eddy simulation. Atmospheric Environment 42, 5885–5895.

Caton, F., Britter, R.E., Dalziel, S.B., 2003. Dispersion mechanism in a street canyon. Atmospheric Environment 37, 693–702.

DePaul, F.T., Sheih, C.M., Noll, K.E., 1985. A tracer study of dispersion in an urban street canyon. Atmospheric Environment 19 (4), 455–459.

Dezso-Weidinger, G., Stitou, A., Van Beeck, J., Riethmuller, M.L., 2003. Measurement of the turbulent mass flux with ptv in a street canyon. Journal of Wind Engineering 91, 1117–1131.

Fackrell, J.E., 1980. A flame ionisation detector for measuring fluctuating concentration. Journal of Physics E: Scientific Instruments 13, 888–893.

Harman, I.N., Barlow, J.F., Belcher, S.E., 2004. Scalar fluxes from urban street canyons. part 2: model. Boundary-Layer Meteorology 113, 387–409.

Hotchkiss, R.S., Harlow, F.H., 1973. Air pollution transport in street canyons. Environmental Protection Agency, 1–128.

Irwin, H.P.A.H., 1981. The design of spires for wind simulation. Journal of Wind Engineering and Industrial Aerodynamics 7, 361–366.

Johnson, W.B., Ludwig, F.L., Dabberdt, W.F., Allen, R.J., 1973. An urban diffusion simulation model for carbon monoxide. Journal of Air Pollution Control Association 23, 490–498.

Kastner-Klein, P., Plate, E.J., 1999. Wind-tunnel study of concentration fields in street canyons. Atmospheric Environment 33 (24–25), 3973–3979.

Kim, J., Baik, J., 2003. Effects of inflow intensity on flow and pollutant dispersion in an urban street canyon. Journal of Wind Engineering and Industrial Aerodynamics 91, 309–329.

Louka, P., Belcher, S.E., Harrison, R.G., 1998. Modified street canyon flow. Journal of Wind Engineering and Industrial Aerodynamics 74–76, 485–493.

Mavroidis, I., Griffiths, R.F., Jones, C.D., Biloft, C.A., 1999. Experimental investigation of the residence of contaminants in the wake of an obstacle under different stability conditions. 33, 939–949.

Meroney, R.N., Pavageau, M., Rafailidis, S., Schatzmann, M., 1996. Study of line source characteristics for 2-d physical modelling of pollutant dispersion in street canyons. Journal of Wind Engineering and Industrial Aerodynamics 62 (1), 37–56.

Narita, K., 2007. Experimental study of the transfer velocity for urban surfaces with a water evaporation method. Boundary-Layer Meteorology 122, 293–320.

de Paula Gomes, M., Isnard, A., do Carmo Pinto, J.M., 2007. Wind tunnel investigation on the retention of air pollutants in three-dimensional recirculation zones in urban areas. Atmospheric Environment 41, 4949–4961.

Salizzoni, P., 2006. Mass and momentum transfer in the urban boundary layer. Ph.D. thesis, Politecnico di Torino – Ecole Centrale de Lyon.

Salizzoni, P., Soulhac, L., Mejean, P., Perkins, R.J., 2008. Influence of a two scale surface roughness on a turbulent boundary layer. Boundary-Layer Meteorology 127 (1), 97–110.

Salizzoni, P., Marro, M., Grosjean, N., Soulhac, L., Perkins, R.J. Turbulent transfer between street canyons and the overlying atmospheric boundary layer. Boundary-Layer Meteorology, submitted for publication.

Salizzoni, P., Van Liefferinge, R., Mejean, P., Soulhac, L., Perkins, R.J., 2009. Influence of wall roughness on the dispersion of a passive scalar in a turbulent boundary layer. Atmospheric Environment 43 (3), 734–748.

Solazzo, E., Britter, R.E., 2007. Transfer processes in a simulated urban street canyon. Boundary-Layer Meteorology 124 (1), 43–60.

Soulhac, L., 2000. Modélisation de la dispersion atmosphérique à l'intérieur de la canopéeurbaine. Ph.D. thesis, Ecole Centrale de Lyon.

Soulhac, L., Mejean, P., Perkins, R.J., 2001. Modelling the transport and dispersion of pollutants in street canyons. International Journal of Environment and Pollution 16 (1–6), 403–413.

Yamartino, R.J., Wiegand, G., 1987. Development and evaluation of simple models for the flow, turbulence and pollutant concentration fields within an urban street canyon. Atmospheric Environment 20 (11), 2137–2156.

Yang, Y., Shao, Y., 2006. A scheme for scalar exchange in the urban boundary layer. Boundary-Layer Meteorology 120, 111–132.